Quasi-Z-Source Indirect Matrix Converter Fed Induction Motor Drive for Flow Control of Dye in Paper Mill

D. Sri Vidhya and T. Venkatesan

***Abstract*—This paper describes a flow control of the dye in the paper mill with the quasi-Z-source indirect matrix converter (QZSIMC) fed induction motor drive. More than a decade the voltage-source inverter (VSI) and current-source inverter (CSI) have been used to control the speed of the induction motor, which in turns controls the flow of dye. Recently, the matrix converter (MC) has been an excellent competitor for the VSI or CSI for its compactness. The voltage transfer ratio of the VSI, CSI, and MC has been limited to 0.866. Thus, the efficiency of these converters is less. To improve the voltage transfer ratio the quasi-Z-source network (QZSN) is to be used between voltage source and indirect MC (IMC). The modification in the shoot-through duty ratio of the QZSN varies the voltage transfer ratio greater than 0.866. Different voltage transfer ratios are needed for different voltage sag conditions. For a variation of the duty ratio of the QZSN, the fuzzy logic controller has been presented. To control the IMC vector control with space vector modulation has been presented. This paper proposes the implementation of QZSIMC adjustable speed drive for the flow control of dye in paper mill during different voltage sag conditions. A 4-kW prototype has been built and the effectiveness of the proposed system is verified with simulation results and experimental setup. Simulation is done in MATLAB, Simulink platform. Experimental setup is done with the aid of a TMS320F2812 (Texas Instrument) processor. The experimental results validate the maintenance of the speed of an induction motor at the set condition, thus controlling the perfect flow of dye in paper manufacturing technology.**

***Index Terms*—Fuzzy logic controller, quasi-Z-source indirect matrix converter (QZSIMC), voltage boost factor, voltage sag, voltage transfer ratio.**

I. Introduction

VARIABLE speed induction motor drive finds its applications in transportation systems, home appliances, paper and textile mills, rolling and cement mills, pumps, lifts, compressors, blowers, elevator, conveyors, crushers, machine tools, robotics, etc., In USA, the Electric Power Research Institute reports that almost 60–65% of power generation is consumed by electric motor drives. In this 75% of electrical motor drives are pump, fan, and compressor-type drives. Most of the pumps and fans in industries are used for fluid flow control. In the conventional flow control method, an induction motor is coupled to the pump and runs at constant speed. This method causes large energy wastage. Speed control of the motor by a converter can save around 20% energy at light load [1].

The most generally utilized ac–ac converter topology in the industry is a traditional dc-link voltage-source converter. DC-link capacitor makes the traditional B2BC bulky and limits service lifetime [2]. Gyugi and Pelly have introduced the ac–ac converter without the dc-link component with forced commutated cyclo-converter [3]. In 1980, Venturini and Alesina introduced the matrix converter (MC) and they provided the comprehensive mathematical background [4]. The most impressive alternative to MC is the B2BC due to its high power density, bidirectional flow of power, reduced harmonics with sinusoidal waveforms, lower volume and weight, unity power factor, extended lifetime, and dependable in hostile conditions [5]. Dual topologies of MC are direct MC (DMC) and indirect MC (IMC). The DMC performs single stage conversion (ac–ac), whereas the IMC performs two stage conversions (ac–dc–ac) without dc-link capacitor. Even though both converters have same characteristics, the DMC operates with complex commutation, whereas the IMC has easy commutation similar to B2BC [6]. Although many researchers have made significant process, penetration of an MC in industry is less because of its limitations [7]. Like the B2BC, the MC has limited voltage transfer ratio as 0.866. The MC cannot short circuit the source and open circuit the load [8].

Much research was carried out to increase the voltage transfer ratio. An effortless method is to connect a transformer between the supply and the load. But then again the bulky transformer affects the compactness of the MC. Another way is to make the MC to operate in the over modulation region [9]. However, in this process, voltage transfer ratio can be increased up to unity. Szcaesniak has proposed a matrix resonant frequency converter that made the voltage transfer ratio greater than unity. But, in this method, synchronization of an MC and resonant source makes the control of matrix resonant frequency converter complex [10]. Peng introduced the Z-source network (ZSN) in the inverter and improves the voltage transfer ratio up to 1.12. The ZSN has an additional advantage that allows short circuit of the source as a consequence commutation becomes straightforward and effortless [11]. Quasi-ZSN (QZSN) further improves the voltage transfer ratio to four to five times [12].

Manuscript received September 27, 2016; revised January 21, 2017; accepted February 19, 2017. Date of publication March 2, 2017; date of current version November 2, 2017. Recommended for publication by Associate Editor D. Vinnikov.

The authors are with the Department of Electrical and Electronics Engineering, K. S. Rangasamy College of Technology, Tiruchengode 637215, India (e-mail: vidhyasriramesh@gmail.com; pramoth99@yahoo.co.uk).

Color versions of one or more of the figures in this paper are available online at http://ieeexplore.ieee.org.

Digital Object Identifier 10.1109/TPEL.2017.2675903

Incorporation of ZSN/QZSN to DMC/IMC, namely Z-source DMC (ZSDMC) and Z-source IMC (ZSIMC) increases the voltage transfer ratio and allows short circuit of the source. An increase in the voltage transfer ratio provides boost capability to ZSMC. In ZSDMC, the ZSN is sandwiched between the source and MC to improve the voltage transfer ratio. The ZSDMC topology allows entirely silicon solution, but still requires difficult commutation. In a ZSIMC, the ZSN can be placed in the ac source side or in the dc link. ZSN/QZSN combined to the IMC's intermediate dc link results in a not entirely silicon solution, which increases its size and inductance and capacitance weight in the dc link [13]–[14]. Integration of ZSN/QZSN into IMC's ac source side has proposed by Shuo [15] and simplifies the commutation. Additional input filters are required to avoid higher order harmonics of source current. Ellabban *et al.* have proposed the modified continuous QZSDMC [16], [17] but it could not avoid the additional input filters. Shuo *et al.* added the continuous QZSN to IMC and developed a new topology called as quasi-Z-source IMC (QZSIMC). This QZSIMC eliminates the extra filter and has high efficiency [18]. But this topology produces higher voltage stress on the capacitor in the QZSN. As the capacitor has 60% of failure rate, the stress on the capacitor reduces the lifetime of the converter [19]. This paper focuses on the discontinuous QZSIMC topology as it provides less voltage stress on the capacitor in the QZSN.

Input source disturbances in QZSIMC have an immediate reflection on the load. The unbalanced input voltages and input voltage sag can result in unwanted output harmonic currents and voltage sag on the load. This can depreciate the performance of QZSIMC. A fuzzy logic based compensation method during unbalanced input voltage condition has improved the output performance of the ZSMC [20]. By controlling the shoot-through (ST) duty cycle, the system can provide the ride through capability to both balanced and unbalanced sags [21]. In [22], voltage sag compensation has been implemented with boosting of output voltage and made in-phase with the input voltage. Almost all the literature have set ST duty ratio *D* as 0.1, 0.15 [14], 0.2 [20], and 0.33 [18] resulting in constant boost. Constant boost is suitable for the system with constant voltage sag. But, in practical application, voltage sag occurs only for short duration and it is not constant. The novelty of this paper is variable boost with fuzzy controller. Variable boost function was achieved in [23] with fuzzy controller only in simulation. But, its simulation results show more fluctuation in the source voltage. In this paper, fuzzy controller mentioned in [23] was tuned and better results in simulation were achieved. Additionally, it has been also compared with PI controller to prove the better performance of the fuzzy controller. The proposed system was implemented in hardware to control the flow of dye in the paper production process. The Seshasayee Paper and Board (SPB) Limited has its own power generation plant in which there is frequent occurrence of voltage sags. In SPB Limited induction motor acquires almost 80% of the adjustable speed drive for different flow controls of materials. This paper focuses on the flow control of dye based on gram per square meter (GSM) of producing paper in the SPB Limited. In this paper, implementation of the PI and fuzzy controller for QZSIMC is done in simulation and fuzzy controller has been implemented in hardware using 4-kW induction motor. In Section II, the novelty of the proposed system and its application in dye pump has been explained. In Section III, topology, working principle of QZIMC-fed induction motor drive and the space vector modulation (SVM) pattern for both rectifier and inverter is elucidated. Section IV elucidates the proposal of a fuzzy logic controller for variable voltage gain. In Section V, the simulation results of the presented fuzzy-based QZSIMC are explained in detailed manner. Section VI presents the experimental implementation and the results of the QZSIMC-fed induction motor with a DSP processor TMS320F2812 (Texas Instrument). In Section VII, the conclusion has been presented.

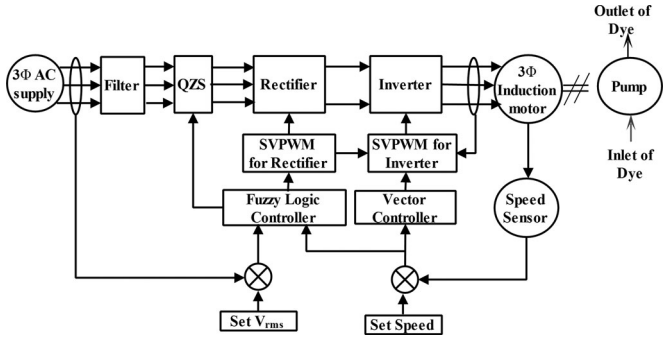

Fig. 1. Block diagram of the proposed fuzzy controller for QZSIMC-fed induction motor drive controlling the dye pump.

II. Proposed QZSIMC With Variable ST Duty Ratio *D* Applied to Dye Pump

The flow of dye depends on the speed of an induction motor. When voltage sag occurs in the supply voltage it affects the speed of an induction motor. To control the flow of dye even under voltage sag conditions, the variable boost QZSIMC with fuzzy controller has been proposed. In this paper, a variable boost capability of the QZSIMC has been tested and analyzed for different voltage sag conditions. Fig. 1 shows the voltage-fed QZSIMC-fed induction motor coupled to dye pump. The topology of QZSIMC has six parts. It has filter, QZSN, rectifier, inverter, induction motor, and dye pump. The PI controller or fuzzy logic controller determines the ST duty ratio *D* of QZSN and rectifier side modulation index m_r. Inverter side modulation index m_{i} of the SVM is controlled with the vector controller. To obtain a controllable input power factor, an SVM technique is required, which modulates the rectifier. At the same time, the output voltage fed SVM is applied to the inverter to modulate the three-phase output voltage.

Fig. 2 shows the storage tank of the dye, a pump connected to the outlet of the tank and the induction motor coupled to the pump. The dye is transferred from the storage tank and mixed with pulp. The mixture is transferred to the head box of the paper machine for the manufacturing of paper. The selected dye pump has flow capacity of 5 L/min for full speed of an induction motor.

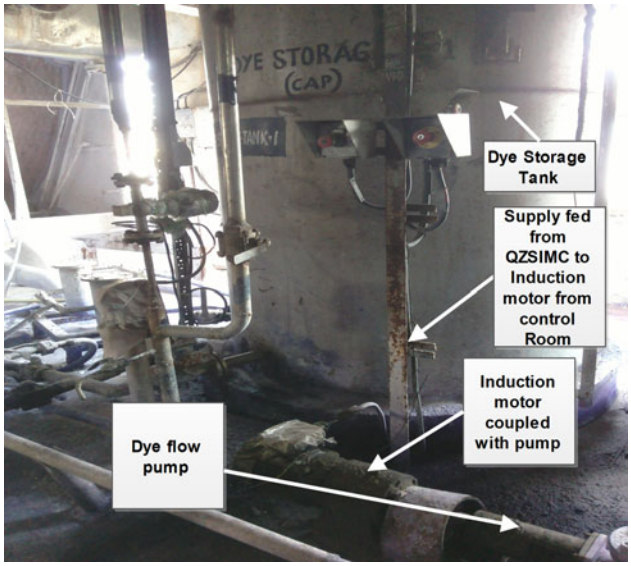

Fig. 2. Real-time connection of the dye storage tank, dye pump, and induction motor.

TABLE I
DYE PUMP (PUMP FLOW CAPACITY 5 L/MIN–100%)

N	% Speed of Induction Motor	% Flow of dye in the pump	GSM of Paper
1	96	100	120
2	70.8	87.2	80
3	60.6	74.5	75
4	48.8	61.6	70
5	36.4	48.1	65
6	22.7	29.1	60

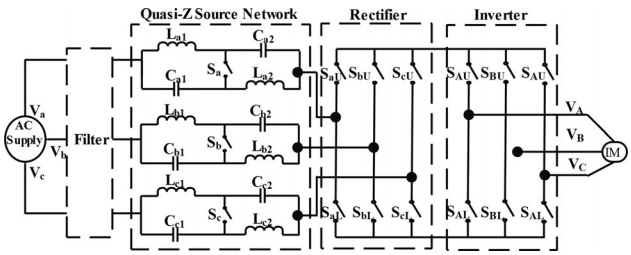

Fig. 3. Topology of voltage-fed QZSIMC-fed induction motor drive.

Table I shows the relation between the GSM, flow of dye, and the speed of induction motor. Flow of pulp, dye, and starch determines the GSM and color shading of the paper. Thus, the accuracy of the flow of materials determines the quality of paper. The proposed system presents the accurate flow of the dye even under different voltage sag conditions.

III. QZSIMC-FED INDUCTION MOTOR DRIVE

A. Topology of the QZSIMC

Fig. 3 shows the topology of the discontinuous QZSIMC-fed induction motor. Two capacitors (C_{x1}, C_{x2}), two inductors (L_{x1}, L_{x2}), and one of bidirectional switches (S_x) have been connected to form QZSN for any one of phase x; $x = a, b, c$.

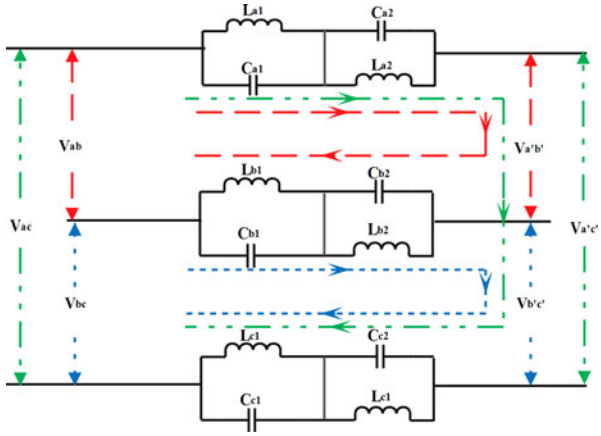

Fig. 4. Equivalent circuit of QZSIMC during NST state.

Similarly, three QZSN has been connected to the three phase supply [24].

B. Operating Principle of the QZSIMC

QZSIMC operates in two states namely non-ST (NST) and ST state. One switching period T_s has NST and ST states. T_{nst} and T_{st} are the time periods of NST and ST states. ST duty ratio is well defined as $D = T_{st}/T_s$. In the NST state, the switches (S_x) are closed. Fig. 4 represents the equivalent circuit of QZSIMC in the NST state. The input voltage of each phase is the sum of the output voltage and the voltage across the two capacitors in each phase as in (1). During this state, the inductor is parallel to the capacitor. Hence, the inductor discharges to the capacitor and the corresponding (2):

$$\begin{bmatrix} V_{ab} \\ V_{bc} \\ V_{ca} \end{bmatrix} = \begin{bmatrix} V_{Ca1} \\ V_{Cb1} \\ V_{Cc1} \end{bmatrix} + \begin{bmatrix} V_{Ca2} \\ V_{Cb2} \\ V_{Cc2} \end{bmatrix} \begin{bmatrix} V_{a'b'} \\ V_{b'c'} \\ V_{c'a'} \end{bmatrix} - \begin{bmatrix} V_{Cb1} \\ V_{Cc1} \\ V_{Ca1} \end{bmatrix} - \begin{bmatrix} V_{Cb2} \\ V_{Cc2} \\ V_{Ca2} \end{bmatrix} \quad (1)$$

$$\begin{bmatrix} V_{Ca1} \\ V_{Cb1} \\ V_{Cc1} \end{bmatrix} = \begin{bmatrix} V_{La1} \\ V_{Lb1} \\ V_{Lc1} \end{bmatrix}, \quad \begin{bmatrix} V_{Ca2} \\ V_{Cb2} \\ V_{Cc2} \end{bmatrix} = \begin{bmatrix} V_{La2} \\ V_{Lb2} \\ V_{Lc2} \end{bmatrix}. \quad (2)$$

In the ST state the switches (S_x) are open and the upper three switches of the rectifier (S_{aU}, S_{bU}, and S_{cU}) are shorted. As the switches (S_{aU}, S_{bU}, and S_{cU}) are closed, the output voltage becomes zero in (1) in the ST state and it can be rewritten as (3). As the switches (S_x) are opened, the inductor charges and its equation are represented as (4):

$$\begin{bmatrix} V_{ab} \\ V_{bc} \\ V_{ca} \end{bmatrix} = \begin{bmatrix} V_{Ca1} \\ V_{Cb1} \\ V_{Cc1} \end{bmatrix} + \begin{bmatrix} V_{Lb2} \\ V_{Lc2} \\ V_{La2} \end{bmatrix} - \begin{bmatrix} V_{Lb1} \\ V_{Lc1} \\ V_{La1} \end{bmatrix} - \begin{bmatrix} V_{Cb2} \\ V_{Cc2} \\ V_{Ca2} \end{bmatrix} \quad (3)$$

$$\begin{bmatrix} V_{Ca1} \\ V_{Cb1} \\ V_{Cc1} \end{bmatrix} + \begin{bmatrix} V_{La2} \\ V_{Lb2} \\ V_{Lc2} \end{bmatrix} = \begin{bmatrix} V_{La1} \\ V_{Lb1} \\ V_{Lc1} \end{bmatrix} + \begin{bmatrix} V_{Ca2} \\ V_{Cb2} \\ V_{Cc2} \end{bmatrix}. \quad (4)$$

Due to the symmetry of QZSN, voltage across the inductor and capacitor is equal and is given as

$$\begin{bmatrix} V_{\mathrm{La2}} \\ V_{\mathrm{Lb2}} \\ V_{\mathrm{Lc2}} \end{bmatrix} = \begin{bmatrix} V_{\mathrm{La1}} \\ V_{\mathrm{Lb1}} \\ V_{\mathrm{Lc1}} \end{bmatrix}, \quad \begin{bmatrix} V_{\mathrm{Ca1}} \\ V_{\mathrm{Cb1}} \\ V_{\mathrm{Cc1}} \end{bmatrix} = \begin{bmatrix} V_{\mathrm{Cb2}} \\ V_{\mathrm{Cc2}} \\ V_{\mathrm{Ca2}} \end{bmatrix}. \quad (5)$$

In the steady state, the average voltage across the inductor and the average current across the capacitor for one switching period should be equal to zero. The voltage boost factor of QZSIMC can be expressed as

$$B_{\mathrm{qz}} = \frac{v_m}{v_i} = \frac{1}{1-2D} \quad (6)$$

where B_{qz} is the voltage boost factor and *D* is ST duty ratio of QZSN. The voltage gain *G* of the proposed QZSIMC is computed by

$$G = B_{\mathrm{qz}} m \quad (7)$$

where $m = m_r\, m_i$ is the modulation index of the IMC, with m_r being the modulation index of the source side rectifier and m_{i} being the modulation index of the load side inverter. From (6), it is evident that the voltage boost factor B_{qz} depends on the ST duty ratio *D*. The voltage gain *G* can be varied by adjusting the ST duty ratio *D*. The voltage gain *G* of the proposed QZSIMC can be greater than unity. It depends on the modulation index *m* and boost factor B_{qz}. The ST duty ratio *D* depends on the modulation index m_r of the rectifier, and for the maximum voltage boost factor it is expressed as [14]

$$D \leq 1 - m_r. \quad (8)$$

From (6)–(8) and assuming m_{i} as unity, voltage gain *G* is expressed as

$$G = \frac{1-D}{1-2D} m_i. \quad (9)$$

C. Design Parameter of QZSN

Inductor voltage and capacitor current can be written as

$$V_L = L\Delta i_L \quad \text{and} \quad i_c = c\Delta V_c. \quad (10)$$

During the NST state, the capacitor voltage is equal to the inductor voltage and during the ST state the capacitor current is equal to the inductor current. Thus, the change in the inductor current and the change in the capacitor voltage can be written as

$$\Delta i_L = \frac{V_c T_{\mathrm{nst}}}{L} \quad \text{and} \quad \Delta V_c = \frac{i_L T_{\mathrm{st}}}{C}. \quad (11)$$

Using (1)–(6), the change in the inductor current and the change in the capacitor voltage can be written as

$$\Delta i_L = \frac{D}{2D-1} \frac{(1-D)T_s}{L} V_i \text{ and } \Delta V_c = \frac{1-D}{1-2D} \frac{DT_s}{C} i_i \quad (12)$$

where V_{i} and i_{i} are the voltage and current of the voltage source, respectively. The designed inductor current ripple ratio r_{i} and capacitor voltage ripple ratio $r_{\mathrm{c}}$are 0.25 and 0.05, respectively. As $\Delta i_{\mathrm{L}} < r_{\mathrm{i}} i_{\mathrm{L}}$ and $\Delta V_c < r_{\mathrm{c}} V_{\mathrm{c}}$, the designed inductor and capacitor are given by

$$L \geq \frac{DT_s\,|Z|}{r_i m} \text{ and } C \geq \frac{(1-D)mT_s}{r_c\,|Z|} \quad (13)$$

where *Z* is the load impedance. While assuming that the voltage source is having unit power factor, $i_i\,|Z| = V_i m$.

TABLE II
INPUT CURRENT VECTOR, SWITCHING COMBINATIONS, AND DC-LINK VOLTAGE

N	Vector	S_{ap}	S_{bp}	S_{cp}	S_{an}	S_{bn}	S_{cn}	V_{dc} (DC-Link Voltage)
1	I_1	1	0	0	0	0	1	V_{ac}
2	I_2	0	1	0	0	0	1	V_{bc}
3	I_3	0	1	0	1	0	0	$-V_{\mathrm{ab}}$
4	I_4	0	0	1	1	0	0	$-V_{\mathrm{ac}}$
5	I_5	0	0	1	0	1	0	$-V_{\mathrm{bc}}$
6	I_6	1	0	0	0	1	0	V_{ab}
7	I_{d}	1	1	1	0	0	0	0
8	I_{d}	0	0	0	1	1	1	0
9	I_0	1	0	0	1	0	0	0
10	I_0	0	1	0	0	1	0	0
11	I_0	0	0	1	0	0	1	0

D. Space Vector Modulation

In the rectifier switch mode, there are two operating states, namely active vector and zero vector states. In order to realize boost voltage in the QZSN, ST is being inserted in the zero vector state, which is shown in Table II. In order to obtain boost voltage output during the ST state, three-phase ac supply is short circuited [25].The SVM vector time periods are calculated by

$$\left.\begin{aligned} T_\alpha &= m_r \sin\left(\tfrac{\pi}{3} - \theta_r\right) T_s \\ T_\beta &= m_r \sin\left(\theta_r\right) T_s \\ T_{\mathrm{st}} &= \mathrm{const}\left(T_{\mathrm{st}} \leq T_s - T_\alpha - T_\beta\right) \\ T_{\mathrm{zr}} &= T_s - T_\alpha - T_\beta - T_s \end{aligned}\right\} \quad (14)$$

where m_r is the modulation index of the source side rectifier, θ_r is the input current vector angle, and $T_\alpha, T_\beta, T_{\mathrm{st}}$, and T_{zr} are the time periods of different current vectors.

The load side inverter that is the similar to a conventional voltage-source inverter has six active vectors and two zero vectors, and the ST duty ratios are calculated by

$$\left.\begin{aligned} T_\rho &= m_i \sin\left(\tfrac{\pi}{3} - \theta_i\right) T_s \\ T_\sigma &= m_i \sin\left(\theta_i\right) T_s \\ T_{\mathrm{zi}} &= T_s - T_\rho - T_\sigma \end{aligned}\right\} \quad (15)$$

where m_i is the modulation index of the load side inverter and T_ρ, T_σ and T_{zi} are the time periods of output voltage active vector and zero vectors, respectively.The modulation pattern combines both the rectification and inversion switching states to obtain an effective balance of the input currents and output voltages in the switching period. The corresponding ST duty ratios can be calculated as

$$\left.\begin{aligned} T_{\rho\alpha} = T_\rho.T_\alpha, T_{\rho\beta} = T_\rho.T_\beta, T_{\sigma\alpha} = T_\sigma.T_\alpha, \\ T_{\sigma\beta} = T_\sigma.T_\beta, T_{\mathrm{zi}\alpha} = T_{\mathrm{zi}}.T_\alpha, T_{\mathrm{zi}\beta} = T_{\mathrm{zi}}.T_\beta. \end{aligned}\right\} \quad (16)$$

where T_s is the switching period,$T_{\rho\alpha}, T_{\rho\beta}, T_{\sigma\alpha}, T_{\sigma\beta}, T_{\mathrm{zi}\alpha}$ and $T_{\mathrm{zi}\beta}$ are the switching periods of different output voltage

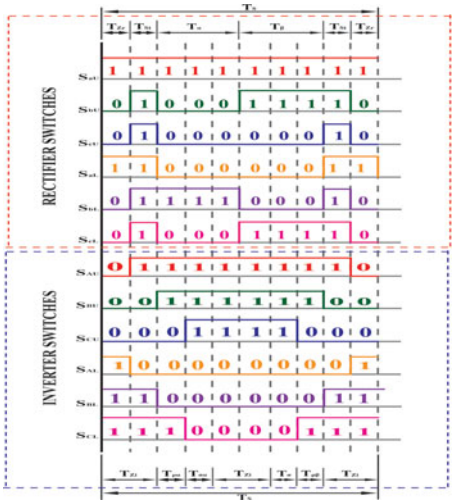

Fig. 5. SVM switching sequence with insertion of ST.

vectors in single switching period T_s. The switching pattern is shown in Fig. 5 for both rectifier and inverter with zero current commutation.

IV. Control Scheme Based on Fuzzy Logic Controller (FLC)

In QZSIMC, both the boost factor *B* and the gain *G* depend on the modulation index (*m*) and ST duty ratio *D*. The constant modulation index (*m*) and ST duty ratio *D* is appropriate for the balanced source, constant load, and constant speed operation. Modulation index $m = m_{\mathrm{r}} \cdot m_{\mathrm{i}}$.

A. Control Scheme for an Inverter

The vector controller provides control action over the outer speed loop and inner current loop with its *q*-axis component and *d*-axis component thereby providing error-free speed tracking. The vector controller fixes the modulation index (m_{i}) of the load side inverter. When there is a drop in input voltage, the dc-link voltage is being affected, which thereby affects the performance of the vector controlled inverter-fed induction motor drive. Therefore, dc-link voltage plays a major role in the performance of the QZSIMC. QZSN and source side rectifier decide the dc-link voltage. Furthermore, PI and fuzzy logic controllers are implemented to optimize ST duty ratio *D* and source side rectifier modulation index (m_{r}), thereby deciding the gain (*G*) of the QZSN.

B. PI Controller for a Rectifier

Simple proposal and integral controller have been implemented to decide the ST duty ratio *D* and source side rectifier modulation index (m_{r}) based on the input voltage sag conditions. Error in the input voltage and change in error in the input voltage are fed as input variable to the PI controller. ST duty ratio *D* is the output variable of the PI controller. Using PI tuner in the MATLAB–Simulink software, the gain of the controller was tuned with Ziegler–Nichols method, which robustly stabilizes the system.

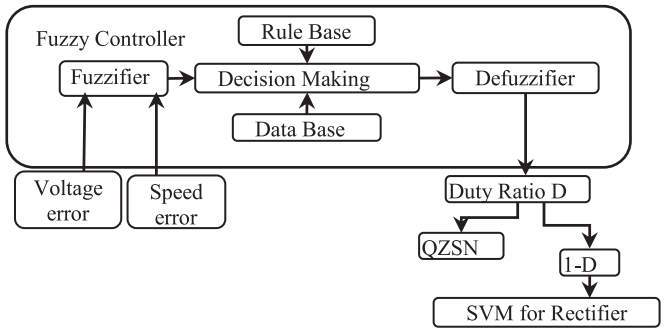

Fig. 6. Structure of a fuzzy logic controller.

TABLE III
Fuzzy Set Linguistic Terms

Parameter	Fuzzy Set	Expression
Input	NB	Negative big
	NS	Negative small
	Z	Zero
	PS	Positive small
	PB	Positive big
Output	VL	Very low
	L	Low
	M	Medium
	B	Big
	VB	Very Big

C. Fuzzy Logic Controller for a Rectifier

A fuzzy logic controller structure is shown in Fig. 6.

The design steps are as follows.

Step 1: Initial step is to set the inputs and outputs variables. The input variables that are considered are the input voltage error and speed error. The output variable, ST duty ratio *D* is being considered.

Step 2: Fuzzification forms the process of converting the input from numerical or crisp value into fuzzy values and the outputs from fuzzy value to crisp value. For the conversion process of crisp values to linguistic terms, fuzzy membership functions are used. A fuzzy variable contains many fuzzy subsets that depend on the number of linguistic terms used. Each of the fuzzy subsets represents one linguistic term that allows its members to have different grades of membership, whereby the membership value lies in the interval [0, 1]. Linguistic values chosen for input and output variable are represented in Table III.

Step 3: This step defines fuzzy membership functions. Based on the designer's preference and experience, the shape of the fuzzy membership function is defined. The triangular shape has been chosen as it provides easy representation, less computation time, and damping of oscillation. Triangular input and output membership function are selected from the defined range, as shown in Fig. 7.

The universe of discourse for a fuzzy logic controller is normalized between $[-4, 4]$ for input and between [0, 0.5] for output. Linguistic variables NB and PB for inputs are made left open and right open to incorporate the negative infinite and positive infinite values. Thus, two input scaling factors namely

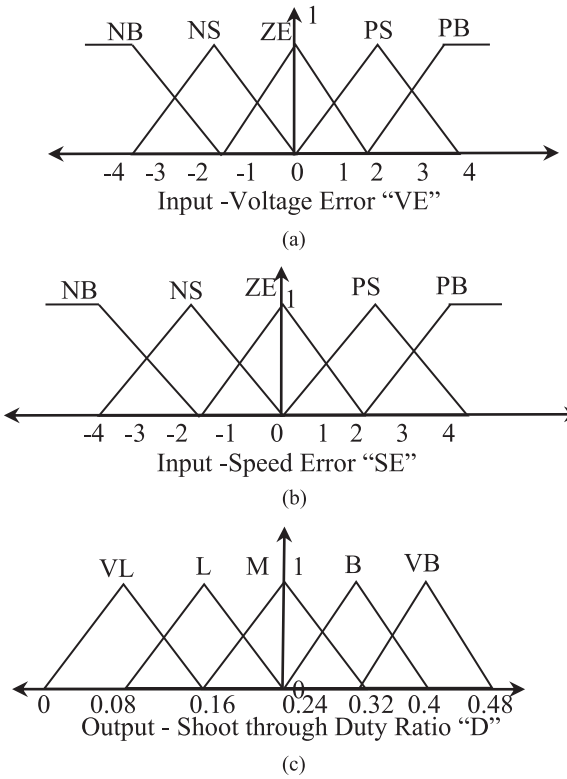

Fig. 7. Membership function. (a) Input-voltage error "VE," (b) input-speed error "SE," and (c) output-ST duty ratio "D."

VE and SE and one output scaling factor namely D have to be designed. Input supply voltage to the system is sinusoidal 230 V. Thus, the possible input voltage error range is from −230 to 230 voltages. Thus, voltage error range [−160,160] has been scaled down to [−4, 4] from NS to PS. The range of the NB has been chosen from −230 to −160 with left open and the range of the PB has been chosen from 160 to 230 with right open. The rated speed of the induction motor is 1500 r/min. The possible error range is from −1500 to 1500 r/min. To achieve minimum speed error the speed error from −50 to 50 has been scaled as −4 to 4 for NS to PS. The range of the NB has been chosen from −1500 to −25 with left open and the range of the PB has been chosen from 25 to 1500 with right open. The range of the ST duty ratio has been limited below 0.5. Thus, the range of the ST duty ratio *D* has been selected from 0 to 0.5.

Step 4: This step defines the rules for selected membership function. In this case, FLC utilizes fuzzy rules instead of using a mathematical formula in order to make a decision and generate control action. The rules are in the form of if–then statements. For example, if the input voltage error (VE) is negative small (NS) and the speed error (SE) is positive small (PS), then the output is medium (M). A total of 25 rules are framed, as mentioned in Table IV.

Step 5: Finally, the defuzzification process is performed. Conversion of fuzzy output to crisp output forms the defuzzification process. Although many defuzzification methods are available, the most preferred is the centroid method or center of gravity has been implemented as it is very precise and provides smooth

TABLE IV
FUZZY RULES

SE	VE				
	PB	PS	ZE	NS	NB
PB	VL	VL	VL	L	M
PS	VL	VL	L	M	B
ZE	VL	L	M	B	VB
NS	L	M	B	VB	VB
NB	M	B	VB	VB	VB

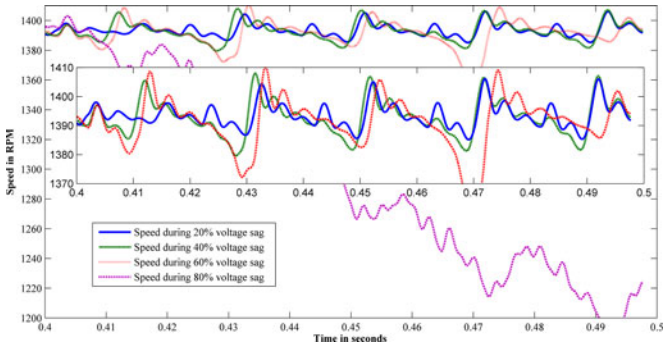

Fig. 8. Speed response of a PI controller at different voltage sag conditions.

output. The formula for the centroid method is given as

$$\text{Centroid} = \frac{\int z\mu_a(z)zdz}{\int z\mu_a(z)dz}. \tag{17}$$

V. Simulation Results and Discussion

Simulation of the QZSIMC is done with MATLAB Version 7.10.0.499 (R2010a) Simulink in Intel (R) Core (TM) i3 CPU M370 @ 2.40 GHz Processor. Simulation is done with a 4-kW induction motor with rating 415 V, 6.5 A, 50 Hz, and 1500 r/min. To compare the speed control capability of PI and fuzzy controller different voltage sag conditions have been applied to the supply voltage at 1400 r/min. Figs. 8 and 9 represent the speed response of PI and fuzzy controller for 20%, 40%, 60%, and 80% voltage sag conditions. Comparison of speed response for PI and fuzzy controller was made and is shown in Fig. 10. From the speed response root mean square error (RMSE), integral time weighted square error (ITSE), and integral time weighted absolute error (ITAE) in r/min have been calculated and tabulated in Table V. It is evident that the all the error in the fuzzy controller was less than the PI controller. Thus, concluding that the speed response of the fuzzy controller was better than the PI controller.

After proving the superior performance of fuzzy controller, four case studies were considered to analyze the performance of the proposed fuzzy logic based QZSIMC-fed induction motor drive for variable boost function. Different voltage sag conditions are selected for case study. Cases 1, 2, 3, and 4 are simulated with 20%, 40%, 60%, and 80% voltage sag conditions after 0.2 s. The response of the proposed variable ST duty ratio *D* based on the input voltage sag and speed error has been

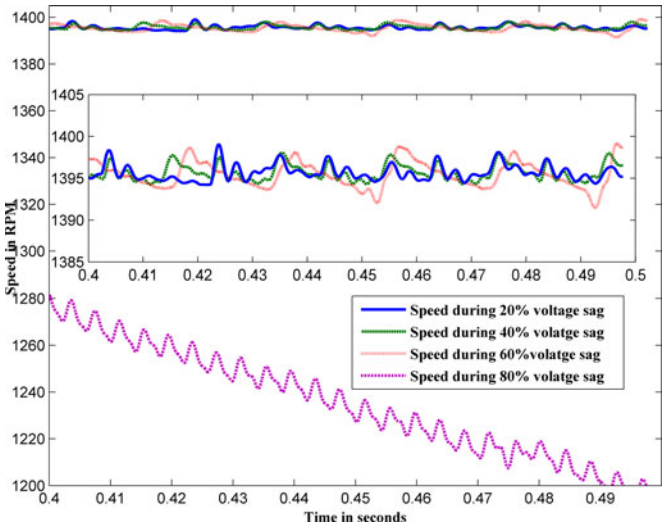

Fig. 9. Speed response of a fuzzy Controller at different voltage sag conditions.

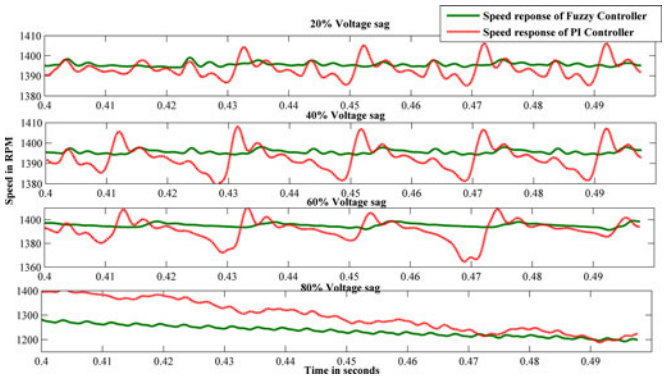

Fig. 10. Comparison of speed responses of PI and fuzzy controllers.

TABLE V
COMPARING PI CONTROLLER AND FUZZY CONTROLLER

Case	PI: RMSE	Fuzzy: RMSE	PI: ITSE	Fuzzy: ITSE	PI: ITAE	Fuzzy: ITAE
Case 1: 20% voltage sag	7.627	2.413	76.528	24.043	8.718	5.374
Case 2: 40% voltage sag	9.428	2.405	112.138	24.069	11.006	5.338
Case 3: 60% voltage sag	12.187	4.794	192.735	30.031	11.976	5.819
Case 4: 80% voltage sag	120.138	80.391	3960.156	221.27	2702.261	722.465

discussed. The induction motor drive is started with no load at a set speed of 1400 r/min.

At 0.1 s, the torque load of 10 N·m has been applied. During starting as the speed error are high, the ST occurs. The duty ratio of the ST pulse slowly reduces from 0.4 to 0.1 with respect to the speed error.When the speed error reaches zero the selection of ST duty ratio becomes zero. The induction motor drive has been started with no load at a set speed of 1400 r/min and after transient at 0.25 s, the load of 10 N·m has been applied.

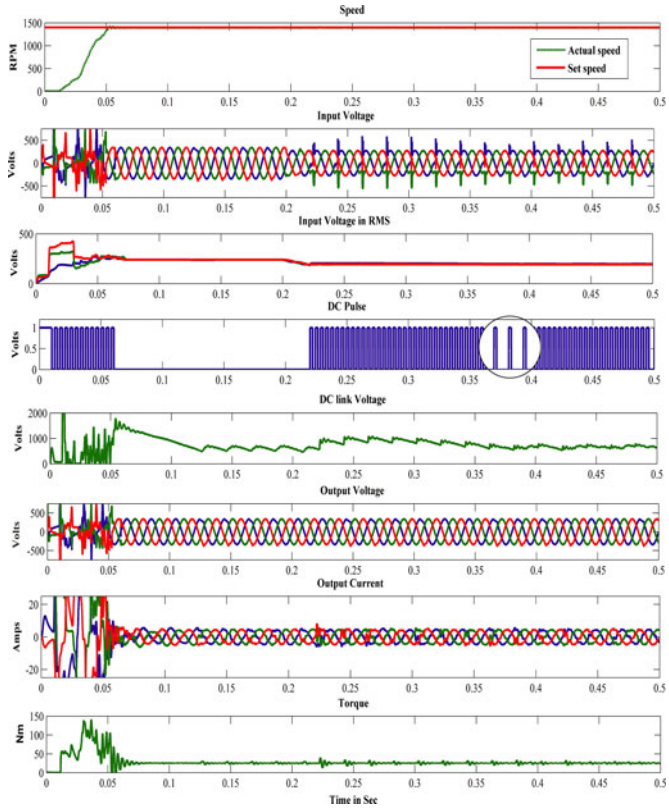

Fig. 11. Case 1: QZSIMC with 20% voltage sag: speed, input voltage, $V_{\rm rms}$ of phase to ground input voltage, dc ST pulse, dc-link voltage output voltage, output current, and torque.

A. Case 1: 20% Voltage Sag

In this case, voltage sag of 20% occurs after 0.2 s, as shown in Fig. 11. The input voltage and $V_{\rm rms}$ voltage represents a voltage drop of 240 to 192 V. The ST pulse starts it firing with a duty ratio of 0.1 after 0.2 s. The dc-link voltage increases as the boosting of voltage is done after 0.2 s to maintain the speed. The speed response, output voltage, output current, and torque even after the 20% voltage sag are very good and the motor speed is maintained at 1400 r/min. Thus, for a 20% voltage sag the proposed system works well.

B. Case 2: 40% Voltage Sag

In this case, voltage sag of 40% occurs after 0.2 s, as shown in Fig. 12.The input voltage and $V_{\rm rms}$ voltage drops from 240 to 144 V the corresponding ST duty ratio also increases to 0.2 from 0.1 when compared to case 1. The dc-link voltage boosted output voltage spiked up to 500 V to maintain the speed. The speed response even after the 40% voltage sag is good. But, there occurs small distortion at 0.22 s. After 0.25 s the motor actual speed quickly recovers and speed is maintained at 1400 r/min.

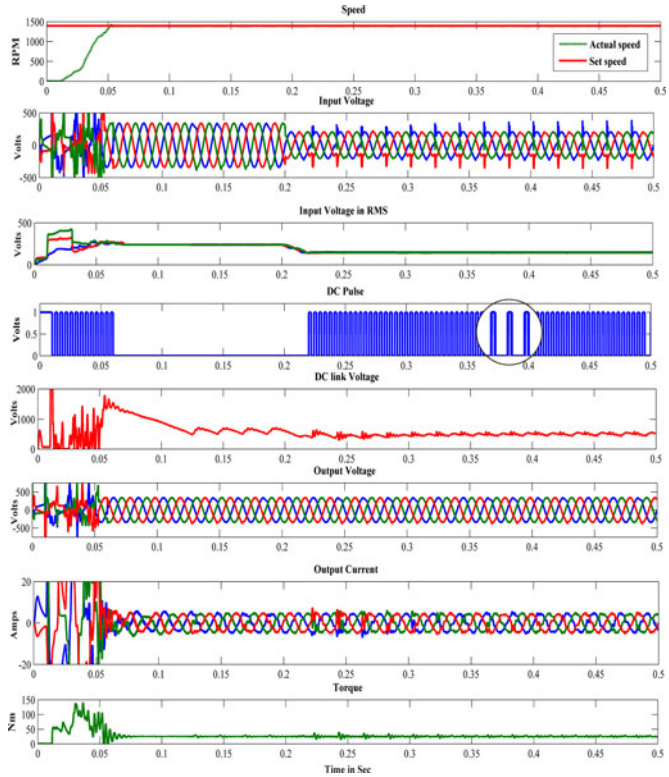

Fig. 12. Case 2: QZSIMC with 40% voltage sag: speed, input voltage, $V_{\rm rms}$ of phase to ground input voltage, dc ST pulse, dc-link voltage output voltage, output current, and torque.

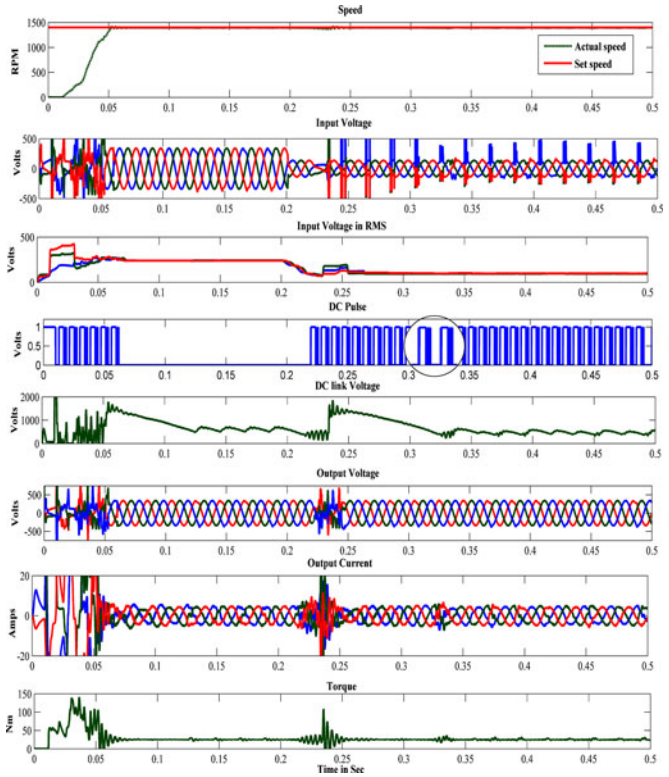

Fig. 13. Case 3: QZSIMC with 60% voltage sag: speed, input voltage, $V_{\rm rms}$ of phase to ground input voltage, dc ST pulse, dc-link voltage output voltage, output current, and torque.

C. Case 3: 60% Voltage Sag

In this case, voltage sag of 60% occurs after 0.2 s, as shown in Fig. 13. The input voltage and $V_{\rm rm}$ voltage drop from 240 to 96 V, the selection of ST duty ratio becomes 0.3 after 0.2 s. At 0.22 s the speed oscillation is higher than case 2 but the speed restores itself after 0.25 s and speed is maintained at 1400 r/min. The dc-link voltage boosted output voltage spiked up to 500 V to maintain the speed.

D. Case 4: 80% Voltage Sag

In this case, voltage sag of 80% occurs after 0.2 s, as shown in Fig. 14. When $V_{\rm rms}$ voltage drop from 240 to 48 V, the selection of ST duty ratio becomes 0.4 after 0.2 s. At 0.22 s the speed oscillation is higher than case 2 but the speed restores itself after 0.25 s and speed could not maintained at 1400 r/min.

VI. Hardware Implementation

Hardware implementation has beed carried out with a 4-kW induction motor as in simulation. Set speed of induction motor has been decided with the required flow of the dye. The flow of the dye is determined from the GSM and shading of paper. Actual speed of the induction motor is measured by the quadrature encoder pulse sensor. The actual speed of induction motor input voltage to the QZSN and the input voltage of induction motor are the parameters fed to the TMS320F2812 DSP processor. Embedded C coding has been used to implement the algorithm

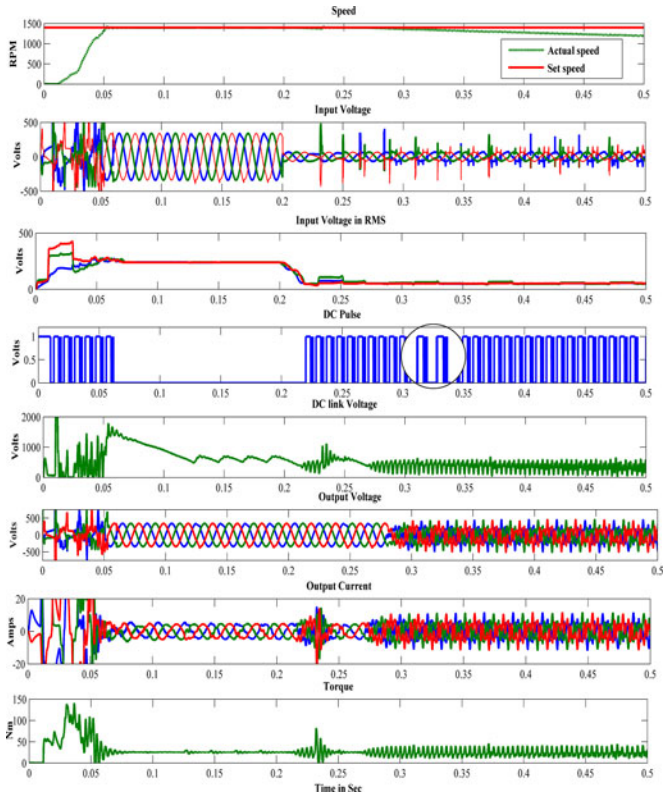

Fig. 14. Case 4: QZSIMC with 80% voltage sag: speed, input voltage, $V_{\rm rms}$ of phase to ground input voltage, dc ST pulse, dc-link voltage output voltage, output current, and torque.

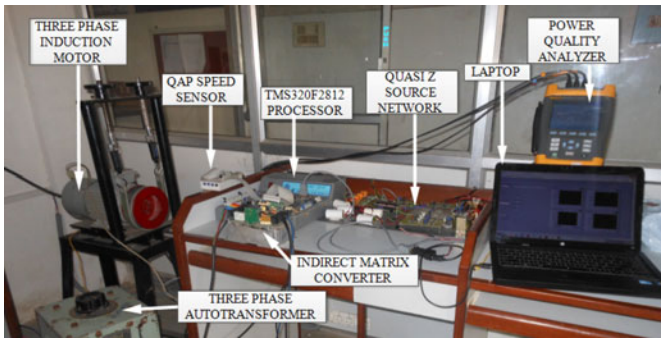

Fig. 15. Experimental setup of a 4-kW prototype for QZIMC-fed induction motor drive.

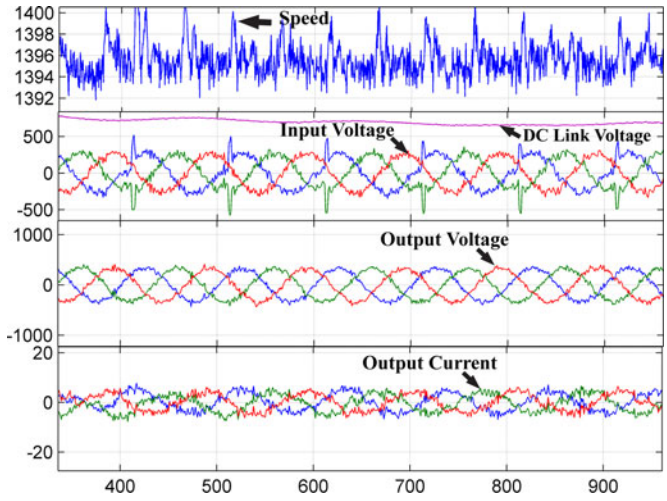

Fig. 16. Experimental results of Case 1: QZSIMC with 20% voltage sag: speed in r/min, dc-link voltage in V, input voltage in V, output voltage in V, and output current in A with *x*-axis time as 20 ms/div.

for the fuzzy controller and the SVPWM. The program for generation of gate pulses for QZSN, rectifier, and inverter has been loaded into a DSP processor. A snapshot of the experimental setup of the proposed system has been shown in Fig. 15.

Figs. 16–19 represent experimental results of case 1 with 20% voltage sag, case 2 with 40% voltage sag, case 3 with 60% voltage sag, and case 4 with 80% voltage sag, respectively. Figs. 16–19 show the experimental results of speed, dc-link voltage, output voltage, and output current for all the cases. From Figs. 16–18, it is evident that the speed of induction motor has been maintained at 1400 r/min with a tolerance of 2%. The speed of the induction motor drops from 1400 to 1200 r/min for 80% voltage drop as evident from Fig. 19. DC-link voltage was maintained at 650 V for 20% voltage sag from Fig. 16. DC-link voltage was maintained at 500 V for both 40% and 60% voltage sags from Figs. 17 and 18. But for the 80% voltage drop the dc-link voltage oscillate from 0 to 600 V, as shown in Fig. 19. For better understanding of the experimental results, comparison of all the cases was made in Table VI. Based on the error in the speed of the induction motor the error in the flow of dye pump occurs. The percentage error in the flow of dye in the dye pump

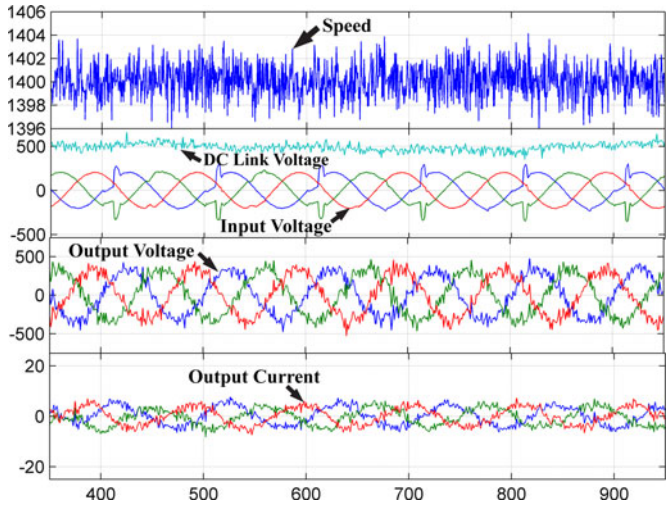

Fig. 17. Experimental results of Case 3: QZSIMC with 40% voltage sag: speed in r/min, dc-link voltage, input voltage in V, output voltage in V, and output current in A with *x*-axis time as 20 ms/div.

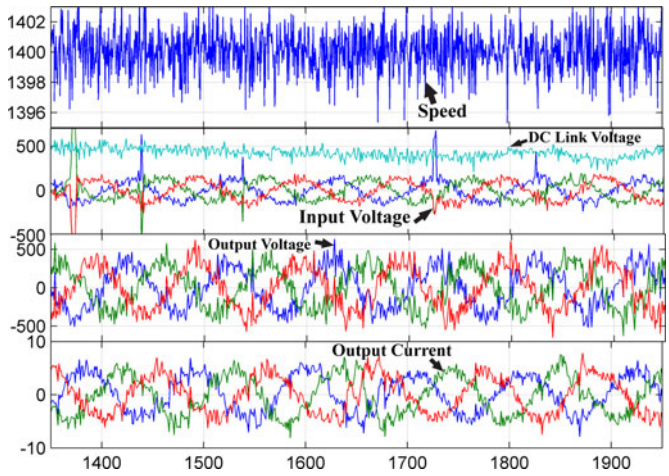

Fig. 18. Experimental results of Case 2: QZSIMC with 60% voltage sag: speed in r/min, dc-link voltage in V, input voltage in V, output voltage in V, and output current in A with *x*-axis time as 20 ms/div.

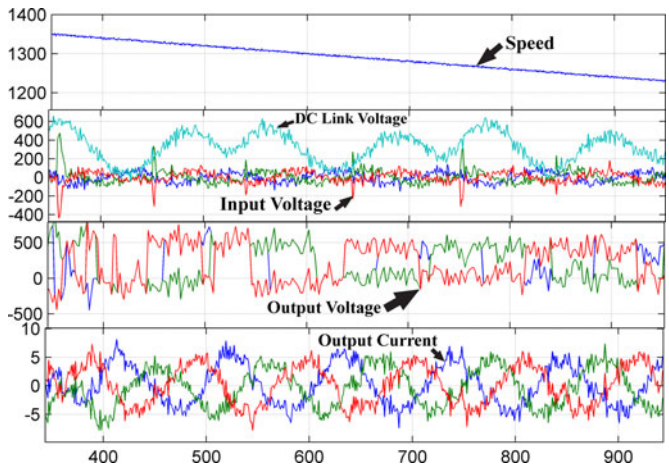

Fig. 19. Experimental results of Case 4: QZSIMC with 80% voltage sag: speed in r/min, dc-link voltage in V, input voltage in V, output voltage in V, and output current in A with *x*-axis time as 20 ms/div.

TABLE VI
COMPARATIVE RESULT ANALYSIS FOR SIMULATION AND EXPERIMENTAL RESULTS FOR VARIOUS VOLTAGE SAGS

Sl No.	Parameter		20% Voltage Sag	40% Voltage Sag	60% Voltage Sag	80% Voltage Sag
1	V_{rms} Input phase to ground Voltage of phase A		240–192 V	240–144 V	240–96 V	240–48 V
2	RMSE for speed response	Simulation	7.62	9.42	12.18	120.13
		Experiment	9.254	11.50	14.53	148.56
3	Mean dc-link voltage	Simulation	680.50	668.71	579.63	324.21
		Experiment	654.54	512.45	498.54	300
4	Percentage flow error		2.1%	2.4%	3.1%	12.5%

for a set flow of 40 m^3 volume of dye was tabulated in Table VI. It is evident that the error is within the prescribed limit of 5% for 20%, 40%, and 60% voltage sags. For 80% voltage sag error reaches 12%.

VII. CONCLUSION

In this paper, based on the fuzzy logic controller, a variable ST duty ratio has been proposed for QZSIMC-fed induction controlling the dye pump and it has been compared with a PI controller. Analysis for RMSE, ITSE and, ITAE was made for speed response of PI controller and fuzzy controller for different voltage sag conditions. Simulation results indicate that the proposed fuzzy controller has better speed response than the PI controller. Positive results were achieved in both simulation and experimental setups for 20%, 40%, and 60% voltage sag. The evaluation of percentage flow error in flow of dye was done with the proposed fuzzy based QZSIMC. The results shows that for 20%, 40%, and 60% voltage sag the percentage flow error is within the limit.

ACKNOWLEDGMENT

The authors gratefully acknowledge the technical support given by Er. N. Narayanasamy, Executive (Electrical), and Er. M. K. Ramesh, J. M (Electrical), Seshasayee Paper and Board Limited, Erode, Tamil Nadu, India. The authors would also like to acknowledge the technical support given by Dr. C. Muniraj, Associate Professor, Department of Electrical and Electronics Engineering, K. S. Rangasamy College of Technology, Tiruchengode, India. The authors acknowledge the financial support from management, K. S. Rangasamy College of Technology.

REFERENCES

[1] B. K. Bose, "Global energy scenario and impact of power electronics in 21st century," *IEEE Trans. Ind. Electron.*, vol. 60, no. 7, pp. 2638–2651, Jul. 2013, doi: 10.1109/TIE.2012.2203771.

[2] J. W. Kolar, T. Friedli, J. Rodriguez and P. W. Wheeler, "Review of three-phase PWM AC–AC converter topologies," *IEEE Trans. Ind. Electron.*, vol. 58, no. 11, pp. 4988–5006, Nov. 2011.

[3] L. Gyugi, and B. Pelly, *Static Power Frequency Changers, Theory, Performance and Application*. New York, NY, USA: Wiley, 1970.

[4] A. Alesina and M. G. B. Venturini, "Analysis and design of optimum-amplitude nine-switch direct AC-AC converters," *IEEE Trans. Power Electron.*, vol. 4, no. 1, pp. 101–112, Jan. 1989.

[5] T. Friedli, J. W. Kolar, J. Rodriguez and P. W. Wheeler, "Comparative evaluation of three-phase AC–AC matrix converter and voltage DC-link back-to-back converter systems," *IEEE Trans. Ind. Electron.*, vol. 59, no. 12, pp. 4487–4510, Dec. 2012.

[6] P. W. Wheeler, J. Rodriguez, J. C. Clare, L. Empringham, and A. Weinstein, "Matrix converters: A technology review," *IEEE Trans. Ind. Electron.*, vol. 49, no. 2, pp. 276–288, Apr. 2002.

[7] L. Empringham, J. W. Kolar, J. Rodriguez and P.W. Wheeler, and J. C. Clare, "Technological issues and industrial application of matrix converters: A review," *IEEE Trans. Ind. Electron.*, vol. 60, no. 10, pp. 4260–4271, Oct. 2013.

[8] J. Rodriguez, M. Rivera, J. W Kolar, and P. W. Wheeler, "A review of control and modulation methods for matrix converters," *IEEE Trans. Ind. Electron.*, vol. 59, no. 1, pp. 58–70, Jan. 2012.

[9] Y. Tamai, H. Ohguchi, I. Sato, A. Odaka, H. Mine, and J. I. Itoh, "A novel control strategy for matrix converters in over-modulation range," in *Proc. Power Convers. Conf.*, Nagoya, Japan, Apr. 2007, pp. 1049–1055.

[10] Paweł Szcześniak, *Three-Phase AC-AC Power Converters Based on Matrix Converter Topology: Matrix-Reactance Frequency Converters Concept*. London, U.K.: Springer-Verlag, 2013.

[11] F. Z. Peng "Z-source inverter," *IEEE Trans. Ind. Appl.*, vol. 39, no. 2, pp. 504–510, Apr. 2003.

[12] J. Anderson and F. Z. Peng, "Four quasi-Z-source inverters," in *Proc. IEEE Power Electron. Spec. Conf.*, Rhodes, Greece, Jun. 2008, pp. 2743–2749.

[13] G. Baoming, L. Qin, W Qian, and F. Zheng Peng, "A family of Z-source matrix converters," *IEEE Trans. Ind. Electron.*, vol. 59, no. 1, pp. 35–46, Jan. 2012.

[14] L. Shuo, G. Baoming, H. Abu-Rub , J. Xinjian, and F. Z. Peng, "A novel indirect quasi-Z-source matrix converter applied to induction motor drives," in *Proc. 2013 IEEE Energy Convers. Congr. Expo.*, Sep. 15–19, 2013, pp. 2440–2444.

[15] L. Shuo, G. Baoming, Y. Xuyang, J. Xinjian, H. Abu-Rub, and F. Z. Peng "A novel quasi-Z-source indirect matrix converter," *Int. J. Circuit Theory Appl.*, vol. 43, pp. 438–454, 2013.

[16] O. Ellabban, H. Abu-Rub, and G. Baoming, "Field oriented control of an induction motor fed by a quasi-Z-source direct matrix converter," in *Proc. 39th Annu. Conf. IEEE Ind. Electron. Soc.*, Nov. 2013, pp. 4850–4855.

[17] O. Ellabban, H. Abu-Rub, and G. Baoming, "A Quasi-Z-Source direct matrix converter feeding a vector controlled induction motor drive," *IEEE J. Emerg. Sel. Topics Power Electron.*, vol. 3, no. 2, pp. 339–348, Jun. 2015.

[18] L. Shuo, G. Baoming, J. Xinjian, H. Abu-Rub, and F. Z. Peng, "Comparative evaluation of three Z-source/quasi-Z-source indirect matrix converters," *IEEE Trans. Ind. Electron.*, vol. 62, no. 2, pp. 692–701, Feb. 2015.

[19] P. Szcześniak, J. Kaniewski, and M. Jarnut, "AC–AC power electronic converters without DC energy storage: A review," *Energy Convers. Manage.*, vol. 92, no. 1, pp. 483–497, Mar. 2015.

[20] K. Park, K. B. Lee, and F. Blaabjerg, "Improving output performance of a Z-source sparse matrix converter under unbalanced Input-Voltage conditions," *IEEE Trans. Power Electron.*, vol. 27, no. 4, pp. 2043–2054, Apr. 2012.

[21] B. Yu, X. Ding, Y. Lu, H. Li, and X. Li, "Voltage sags on Quasi-Z-source adjustable-speed drives system," in *Proc. IEEE Int. Conf. Mechatronics Autom.*, Beijing, China, Aug. 7–10, 2011, pp. 1899–1904.

[22] M. K. Nguyen, Y. G. Jung, and Y. C. Lim, "Single-phase AC–AC converter based on quasi-Z-source topology," *IEEE Trans. Power Electron.*, vol. 25, no. 8, pp. 2200–2210, Aug. 2010.

[23] D. Sri Vidhya, T. Venkatesan, and N. Kanagaraj, "Fuzzy logic controller for variable boost function in quasi Z source indirect matrix converter during voltage sag condition" *Int. J. Fuzzy Syst.*, 2016, doi: 10.1007/s40815-016-0221-x.

[24] L. Shuo, G. Baoming, H. Abu-Rub, J. Xinjian, and F. Z. Peng, "Modeling, analysis, and motor drive application of quasi-Z source indirect matrix converter" *Int. J. Comput. Math. Electr. Electron. Eng.*, vol. 33, no. 12, pp. 298–319, 2014.

[25] L. Xiong, L. PohChiang, W. Peng, and H. Xiaoqing, "Improved modulation schemes for indirect Z-source matrix converter with sinusoidal input and output waveforms," *IEEE Trans. Power Electron.*, vol. 27, no. 9, pp. 4039–4050, Sep. 2012.

D. Sri Vidhya was born in Chitoor, India, in 1982. She received the B.E degree in electrical and electronics engineering from the Bannari Amman Institute of Technology, Sathyamangalam, India, in 2004, and the M.E. degree in power electronics and drives from the K. S. Rangasamy College of Technology, Tiruchengode, India, in 2008. She is currently working toward the Ph.D degree in electrical engineering at Anna University, Chennai, India.

She is currently an Assistant Professor in the K. S. Rangasamy College of Technology. She has published more than 15 research papers in international journals and conferences. Her research interests include induction motor drives, matrix converters, and intelligent techniques.

T. Venkatesan was born in Salem, India, in 1971. He received the B.E. degree in electrical and electronics engineering from the Regional Engineering College, Tiruchirapalli, India, in 1997, the M.E. degree in power system engineering from Annamalai University, Chidambaram, India, in 2002, and the Ph.D. in electrical engineering from Anna University, Chennai, India, in 2013.

He is currently a Professor in the K. S. Rangasamy College of Technology, Tiruchengode, India. He has published more than 33 research papers in international journals and conferences. His research interests include economic dispatch, unit commitment problem solution using soft computing techniques, renewable energy sources, induction motor drives, and intelligent techniques.